## Society for Mathematical Biology

#### ORIGINAL ARTICLE



# Age-Related Changes to the Immune System Exacerbate the Inflammatory Response to Pandemic H1N1 Infection

Ericka Mochan<sup>1</sup> • T. J. Sego<sup>2</sup> • Bard Ermentrout<sup>3</sup>

Received: 18 December 2021 / Accepted: 22 June 2022 / Published online: 12 July 2022 © The Author(s), under exclusive licence to Society for Mathematical Biology 2022

#### **Abstract**

Age-induced dysregulation of the immune response is a major contributor to the morbidity and mortality related to influenza a virus infections. Experimental data have shown substantial changes to the activation and maintenance of the immune response will occur with age, but it remains unclear which of these many interrelated changes are most critical to controlling the survival of the host during infection. To ascertain which mechanisms are predominantly responsible for the increased morbidity in elderly hosts, we developed an ordinary differential equation model to simulate the immune response to pandemic H1N1 infection. We fit this model to experimental data measured in young and old macaques. We determined that the severity of the infection in the elderly hosts is caused by a dysregulation in the innate immune response. We also simulated CD8<sup>+</sup> T cell exhaustion, a common consequence of chronic and extensive infections. Our simulations indicate that while T cell exhaustion is possible in both age groups, its effects are more severe in the elderly population, as their dysregulated immune response cannot easily compensate for the exhausted T cells. Finally, we explore a therapeutic approach to reversing T cell exhaustion through an inflammatory stimulus. A controlled increase in inflammatory signals can lead to a higher chance of surviving the infection, but excess inflammation will likely lead to septic death. These results indicate that our model captures distinctions in the predominant mechanisms controlling the immune response in younger and older hosts and allows for simulations of clinically relevant therapeutic strategies post-infection.

**Keywords** Mathematical modeling of influenza A virus infection · Immunosenescence

Department of Mathematics, University of Pittsburgh, Pittsburgh, PA 15213, USA



 <sup>⊠</sup> Ericka Mochan edmochan@carlow.edu

Department of Analytical, Physical, and Social Sciences, Carlow University, Pittsburgh, PA 15213, USA

Department of Intelligent Systems Engineering, Indiana University, Bloomington, IN 47408, USA

88 Page 2 of 24 E. Mochan et al.

#### 1 Introduction

Aging is a major factor in the efficacy of the immune response to pathogens. Immunosenescence, the age-induced dysregulation of the immune response, causes changes to both the innate and adaptive responses. Aging is generally accompanied by an elevated basal state of inflammation, termed "inflamm-aging," which is a risk factor for many chronic conditions and a contributor to the increased morbidity and mortality often seen in older individuals (Franceschi et al. 2000a; Shaw et al. 2010). Even conditions that can be mild for most patients, such as seasonal influenza, lead to increased morbidity in elderly patients due to this dysregulation of the immune response (Zhou et al. 2012). In fact, up to 90% of deaths from seasonal flu occur in individuals over 65 years old (Plowden et al. 2004).

The innate immune response is particularly affected by aging. Phagocytic cells, such as macrophages, dendritic cells, and neutrophils, become less effective in clearing pathogens as the host ages. Baseline levels of pro-inflammatory cytokines like interleukin (IL)-1, tumor necrosis factor (TNF), and IL-6 are increased, leading to a constant, nonspecific inflammatory state (Ginaldi et al. 2001). Many of the most common diseases associated with aging, such as Alzheimer's disease, arthritis, and cardiovascular diseases, are associated with increased inflammation (Fulop et al. 2018), and high levels of IL-6 have been shown to be one of the strongest predictors of morbidity and mortality in the elderly (Ginaldi et al. 2001).

The combination of increased baseline inflammation and diminished phagocytic responses causes an increase in tissue damage in elderly hosts. This is compounded by an age-induced dysregulated autophagy response, which leads to accumulation of dysfunctional mitochondria, creating excess reactive oxygen species and increasing cellular damage (Salminen et al. 2012). Immunosenescence has also been shown to affect tissue repair, which is primarily coordinated by immune cells. Communication between these cells is thought to be diminished with aging (Salminen et al. 2012), further dysregulating the immune response.

Both T cell and B cell functions also decline with age, limiting the ability of the individual to respond to novel pathogens or vaccines (Plowden et al. 2004). Failure of the adaptive immune response to clear pathogens from the host can exacerbate disease and inflammation. The number of B cells in the host tends to decrease with time (Meyer 2001), as does the efficacy of some antibodies, though the overall number of antibodies tends to increase with age (Josset et al. 2012) Age-induced thymic involution leads to a diminished number of naïve T cells, impairing the host's ability to defend against novel pathogens (Weksler et al. 1978; Franceschi et al. 2000b)

T cells also tend to experience a persistent and serious state of exhaustion in elderly patients with infection (Moskophidis et al. 1993; Inoue et al. 2014; Baral et al. 2019; Saito et al. 2020). Exhausted T cells have severely limited capacity to perform effector functions, leading to a prolonged and exacerbated infection. T cell exhaustion typically occurs after a persistent immune stimulus, such as a chronic infection, cancer, or sepsis (Inoue et al. 2014; Kahan et al. 2015). While T cell exhaustion can occur in any age group, it is especially serious in the elderly population, where immunosenescence has already weakened the immune response substantially.



To describe these age-induced changes to the immune response, we extended our previous mathematical model of the immune response to respiratory viral infection (Mochan et al. 2021) to include equations for the adaptive immune response with CD8+ T cells and antibodies. We fit this new model to experimental data from young and aged cynomolgus macaques infected with the 2009 pandemic H1N1 strain of influenza A virus (Josset et al. 2012). The data show that aged animals exhibit higher viral titers in both the upper and lower respiratory tracts, and higher hemagglutination inhibition (HI) titers in response to the virus. In addition, aged animals show excess pro-inflammatory cytokines and chemokines at 4 and 7 days post-infection (dpi), including IL-1, IL-6, IL-8, IL-15, and MCP-1. T cell production in the aged macaques was also shown to be higher in bronchoalveolar lavage (BAL) fluid but decreased in the blood.

Together these data suggest that aged macaques experience more severe respiratory disease than the young macaques when infected with identical inocula. We used our ordinary differential equation (ODE) model to identify the mechanisms that vary most with age. We also simulate T cell exhaustion and subsequent treatment with IL-15 in young and old macaques. Our results together describe important age-induced changes to the immune response to viral infection.

#### 2 Results

## 2.1 Overview of Modeling Strategy

## 2.1.1 Mathematical Model

Figure 1 summarizes the interactions represented in our model, and Eqs. (1–11) describe the ODE model presented in this work, adapted from our previous work (Mochan et al. 2021) to explicitly include adaptive and humoral responses using data for CD8<sup>+</sup> T cells and antibody responses. A full description of the equations and parameters is given in the Methods and Materials.

Briefly, the model describes the time-dependent dynamics of the virus replication and clearance in both the upper and lower respiratory tract (denoted by subscripts U and L, respectively). The virus begins in both the upper and lower respiratory tract, as the macaques were initially infected via intraocular, intranasal, and intratracheal routes, to ensure the virus reached both compartments. The virus (V) is taken up by target healthy epithelial cells (H), producing a population of infected cells (I) at rate $\gamma_{HV}$ . Infected cells release additional free virus (parameter $\gamma_V$ ) and sustain the virus population in the host. Free virus is eliminated from both the upper and lower compartments by nonspecific immune clearance, controlled by parameters  $a_{VU}$  and  $a_{VL}$ , respectively; by internalization into epithelial cells, controlled by parameter  $\gamma_{VL}$ ; and by antibodies (A), controlled by parameters  $a_{VU}$  and  $a_{VL}$ . In addition, virus moves up the mucociliary escalator from the lower respiratory to the upper (parameter $\beta$ ), where it is eventually expelled by mechanical clearance.

The presence of the virus and infected cells initiates the immune response. Innate immune responses begin with pro-inflammatory signals (F), which bring immune cells



88 Page 4 of 24 E. Mochan et al.

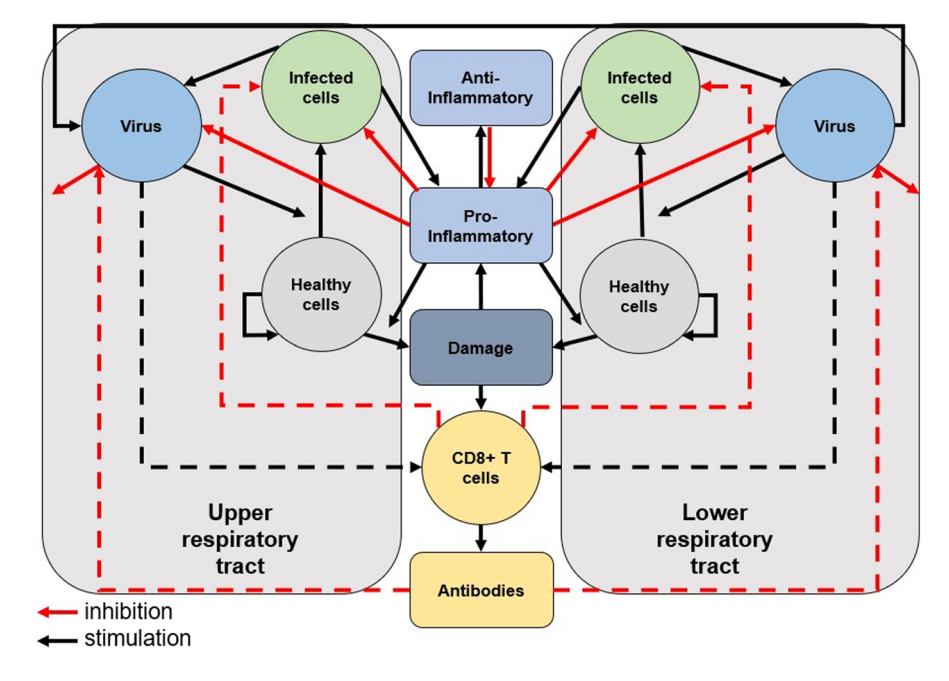


Fig. 1 Network diagram of interactions in the model. Dashed lines represent additional components of the model, adapted from Mochan et al. (Mochan et al. 2021). The model incorporates new mechanisms of the adaptive immune response associated with CD8<sup>+</sup> T cells and antibodies

like macrophages, neutrophils, and natural killer (NK) cells to the site of infection (not included explicitly in the model). These cells can clear infected cells to help control the spread of infection, but also kill healthy epithelial cells in the process (parameter  $a_{HF}$ ), causing damage to the tissue (D). The cells also upregulate more cytokines, such as type I interferon, which can limit the release of free virus from the epithelial cells (parameters  $\kappa_{VFU}$  and  $\kappa_{VFL}$ ).

We have expanded this previous model to include explicit variables and mechanisms representing adaptive immune responses. The virus and cellular damage signals bring CD8<sup>+</sup> T cells (E) to the tissue, and these T cells then clear infected cells (Zajac et al. 1998) (parameter  $a_{1E}$ ). The onset of adaptive immunity also leads to humoral responses, resulting in production of antibodies that eradicate the remaining virus from the host. The variables of this model and the data used to calibrate them are summarized in Table 1. Model parameters are described in Table S1 in Supplemental Materials.

In our previous work (Mochan et al. 2021), we showed that this model could be parameterized to replicate several different possible host immune phenotypes seen in respiratory viral infections: asymptomatic infection, symptomatic survivable infection, lethal infection due to inability to control viral titers, and lethal infection due to excess inflammation and cytokine storm. We now will use the model to demonstrate the host response to infection as it differs between young and older hosts.



Tahla 1	Model	variables	and accordan	ted data fo	r calibration

Variable Name	Description	Data used for calibration from (Josset et al. 2012)
$V_U$	Viral titers in the upper respiratory compartment	Viral genome copy number measured in nasal cavity
$H_U$	Healthy (uninfected) epithelial cells in the upper respiratory compartment	Not calibrated to experimental data
$I_U$	Infected epithelial cells in the upper respiratory compartment	Not calibrated to experimental data
$V_L$	Viral titers in the lower respiratory compartment	Viral genome copy number measured in lungs via bronchoalveolar lavage (BAL)
$H_L$	Healthy (uninfected) epithelial cells in the upper respiratory compartment	Not calibrated to experimental data
$I_L$	Infected epithelial cells in the upper respiratory compartment	Not calibrated to experimental data
F	Pro-inflammatory cytokines	IL-15 (pg/ml)
D	Damage to epithelium	IL-6 (pg/ml)
G	Anti-inflammatory cytokines	Not calibrated to experimental data
E	CD8 <sup>+</sup> T cells	CD8 <sup>+</sup> T cells in BAL
A	Antibodies	Hemagglutination inhibition (HI) titers

## 2.1.2 Ensemble Modeling and Parameter Calibration

To explain the causes of differences in viral host–pathogen interactions between age groups, we fit the model to experimental data from an H1N1 infection of 16 cynomolgus macaques, eight of which were considered young adults, and eight of which were considered aged. All animals from both age groups survived the infection, though the aged animals showed an increased viral load and more severe innate immune responses than the younger animals. In this work, we will use our model to explore differences in these animals' immune responses to better explain why the aged animals experience a more severe infection.

To parameterize the model, we fit model trajectories to viral titers in the upper and lower respiratory tracts, CD8<sup>+</sup> T cells, HI titers (as a proxy for antibody response (Bourgeois and Oaks 2014)), IL-15 (as a proxy for inflammation (Mochan et al. 2021)), and IL-6 (as a proxy for cellular damage (Kopf et al. 1994)). We fit the model parameters to the mean data points for each variable, with their standard deviation. Because ensemble models are meant to represent an entire population, rather than a single individual, we fit the parameters to a mean data point representing the pooled data from macaques. We then use Metropolis–Hastings Monte Carlo sampling, combined with a Bayesian inference approach, to compute a posterior distribution of parameter sets (Mochan et al. 2014; Mochan-Keef et al. 2015; Price et al. 2015). This yields a model ensemble: a large collection of parameter sets which are consistent with the experimental data and coupled with the biological interactions and insights encapsulated in the model equations. Since we are comparing two distinct age groups, we generate



**88** Page 6 of 24 E. Mochan et al.

two distinct parameter distributions, each of which describes the immune response of that population to the viral infection. Some posterior distributions of parameters differ between the adult and aged data: Parameters with large differences between age groups stand out as highly age dependent and largely responsible for the differences seen in the data between younger and older hosts.

## 2.2 Model Trajectory Fits to Experimental Data

## 2.2.1 Ensemble Fits to the Adult (younger) Macague Data

Figure 2 shows the fits to the experimental data for the young adult macaques. All fits from the MCMC procedure predict the virus will be cleared from both compartments within 14 dpi, in accordance with the experimental data. The virus peaks about one order of magnitude higher in the lower compartment than in the upper, as in pandemic strains of H1N1 in human hosts (Yeh et al. 2010). The fraction of infected cells is similarly much higher in the lower compartment than in the upper. Effector T cells become activated around 4 dpi, leading to a quick depletion of the infected cells in both compartments, helping clear the virus from the system. The low number of infected cells in the upper compartment corresponds to minimal upper respiratory symptoms, such as sneezing or runny nose; indeed, experimental observations showed very little symptoms in the infected macaques.

## 2.2.2 Ensemble Fits to the Aged (Older) Macaque Data

Fits to the aged macaque data are shown in Fig. 3. The maximum number of infected cells is slightly lower in the aged simulations than in the young adult simulations. The number of infected cells remains elevated for a longer time in the aged group as well (8 days versus only 5 days in the adult ensembles). This discrepancy corresponds to a longer duration of symptoms in aged hosts, a pattern seen in previous experiments and simulations (Toapanta and Ross 2009; Keef et al. 2017). These results also imply that older hosts exhibit slower clearance of infected cells, which may be caused by a slower reaction of effector cells like NK cells and T cells. Experimental data confirm these patterns, as these cells age, their response rate, and efficacy decline (Toapanta and Ross 2009).

The effects of inflamm-aging can be clearly seen in comparing the ensembles representing younger and older hosts. Inflammation data (IL-15) peak at about 15 pg/mL in the aged macaques, compared to about 11 pg/mL in the adult macaques. Many simulations in the aged macaque ensemble predict the pro-inflammatory cytokines (F) will continue to rise beyond day 4, and the peak will actually occur 1 to 3 days later than in the adult ensemble. The peak is also wider in the older hosts, implying that the inflammation remains elevated for longer as the host ages. Damage also peaks more than twice as high in the older hosts compared to the younger, and the time to reach the peak is about two days longer in the aged hosts.

There is not a substantial age-dependent difference in the CD8<sup>+</sup> T cells in the data, but the tail end of the simulations, where no data guide the fits, shows that T cells are



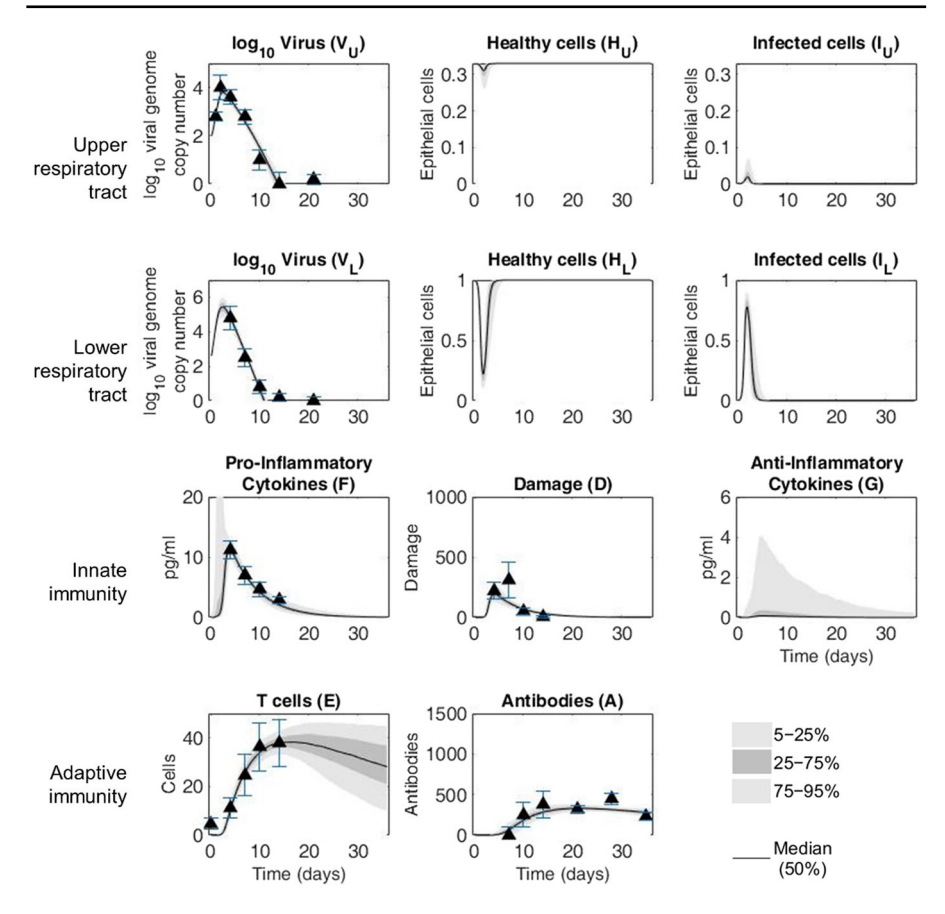


**Fig. 2** Ensemble fits to the adult macaque data. The black line represents the median trajectory, the inner dark gray area represents the 50% confidence interval (25th to 75th percentiles), and the outer light gray envelope represents 90% of the trajectories (5th to 95th percentiles). Trajectories are simulated over five weeks, starting immediately after virus is administered in the nasal cavity (upper respiratory tract) and lungs (lower respiratory tract) at day 0. Experimental data are shown as triangles at the mean with error bars representing standard deviations

predicted to deplete more rapidly in the aged macaques than in the younger. Persistent T cell exhaustion has been shown in elderly hosts in models of sepsis (Inoue et al. 2014) and COVID-19 (Westmeier et al. 2020). Our model predicts a similar behavior after infection with influenza.

Antibody responses peak significantly higher in the aged hosts in both the data and the simulations. Whereas in the younger macaques, the antibody levels reach a peak after about 14 days and remain relatively steady, antibodies in the aged macaques reach a peak after about 21 days and quickly begin to deplete afterwards. By 99 dpi, experimental data show antibodies in both age groups have reached a similar nonzero baseline value (Josset et al. 2012).



88 Page 8 of 24 E. Mochan et al.

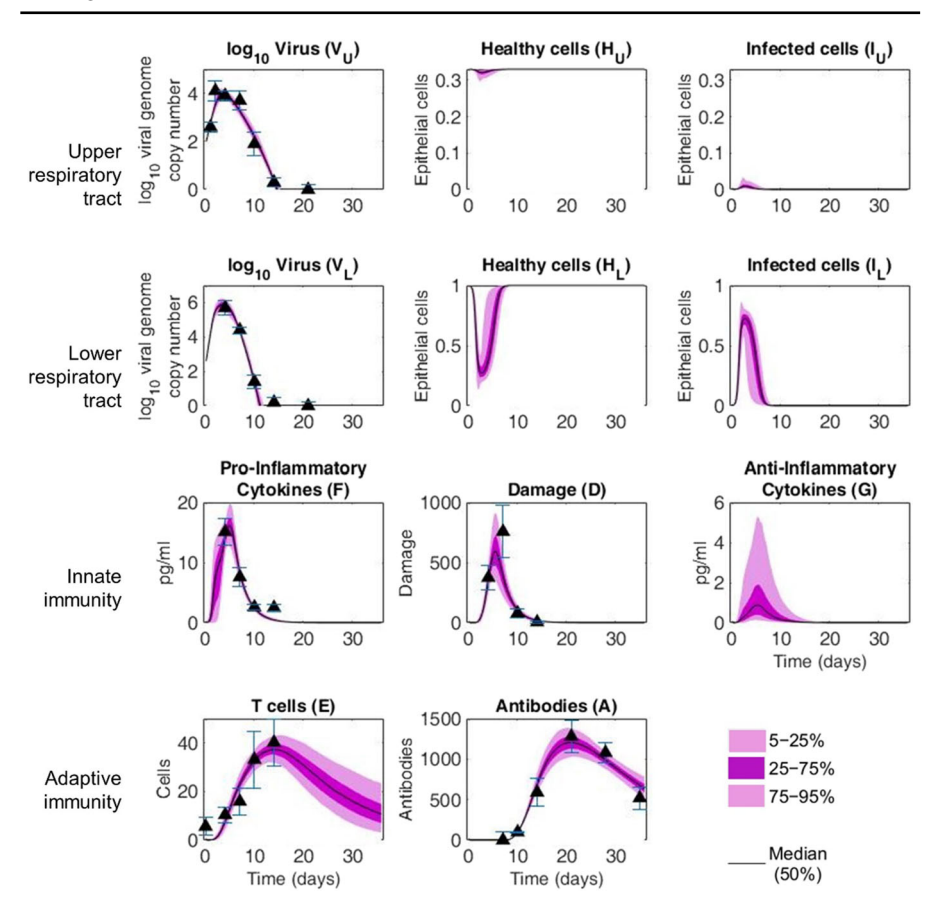


Fig. 3 Ensemble fits to aged macaque data. The black line represents the median trajectory, the inner dark magenta area represents the 50% confidence interval (25th to 75th percentiles), and the outer light magenta envelope represents 90% of the trajectories (5th to 95th percentiles). Trajectories are simulated over five weeks, starting immediately after virus is administered in the nasal cavity (upper respiratory tract) and lungs (lower respiratory tract) at day 0. Experimental data are shown as triangles at the mean with error bars representing standard deviations

## 2.3 Posterior Distributions Explain Age-Related Phenotypes

The marginal distributions calculated in the MCMC procedure reveal the onedimensional distributions of fitted parameters in the model. Because each model parameter represents an amalgamation of interactions and dynamics, and aging affects nearly every aspect of the immune response, we allow all 32 parameters of the model to vary between the two age groups when fitting the data. These distributions show some important trends to understanding the dysregulation of the immune response with age.



## 2.3.1 Aged Animals Exhibit Stronger Pro-Inflammatory Responses

Given the substantial changes in timing and magnitude of innate immune responses that occur during immunosenescence, we hypothesize that the parameters that are key to regulation of the inflammatory response are substantially different between the two age groups. The marginal distributions of parameters comprising the adult (gray) and aged (magenta) ensembles (Fig. 4a) demonstrate that the aged animals have a stronger inflammatory response than the adults. Aged macaques undergo a higher rate of damage to the uninfected epithelial cells (parameter  $a_{HF}$ ), implying that older hosts will experience more tissue damage because of their heightened inflammatory response. Excess tissue damage will likely lead to increased severity in symptoms and morbidity among the elderly individuals (Toapanta and Ross 2009).

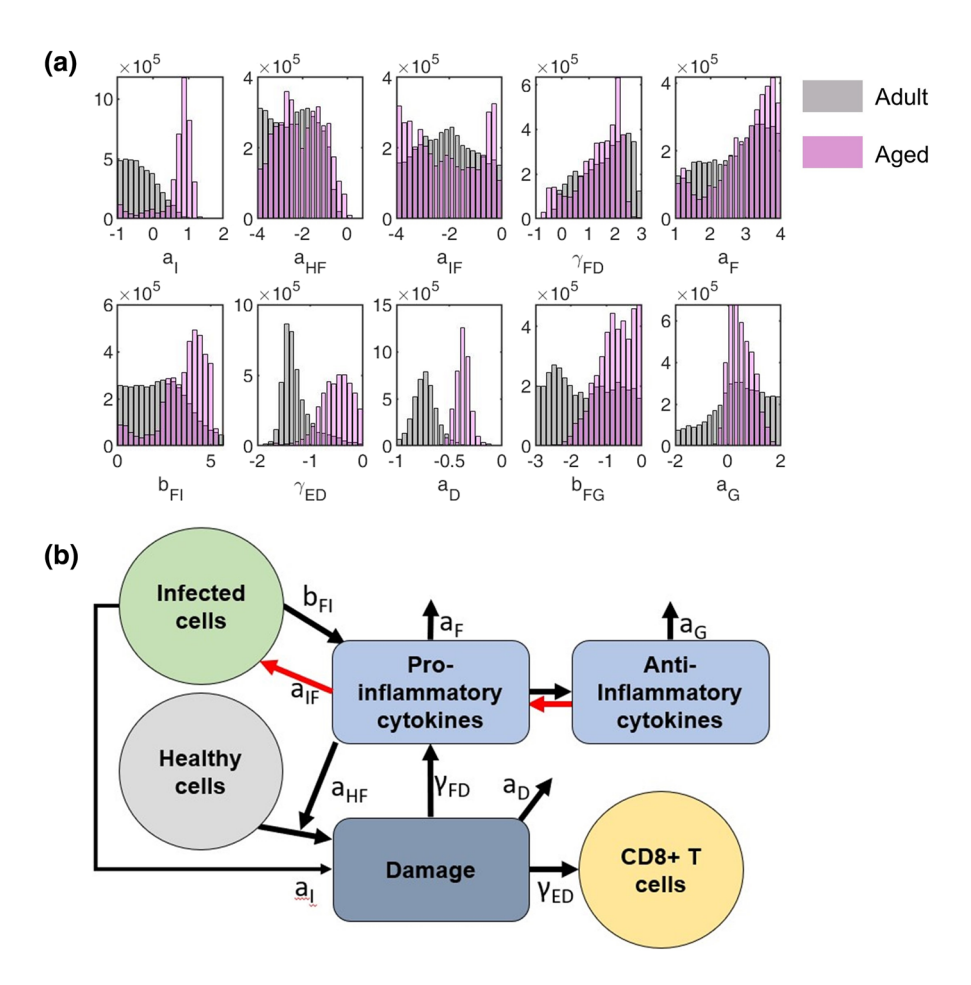


**Fig. 4 a** One-dimensional parameter distributions controlling inflammatory response for adult (gray) vs aged (magenta) macaques. **b** Partial network diagram of inflammation dynamics and interactions in the model. For a full description of the variables and parameters, see Methods and Materials



Infected cells in aged hosts instigate a much stronger inflammatory response than their younger counterparts (parameter  $b_{FI}$ ). The distribution of  $b_{FI}$  is bimodal in the aged macaques; this parameter is negatively correlated with parameter  $\gamma_{FD}$ , which also contributes to the production of inflammation. When one parameter is low, the other will take on a higher value to compensate for its effects. The adult macaques also show an unbalanced bimodality in parameter  $\gamma_{FD}$ . The peak at higher values of  $\gamma_{FD}$  in the adult simulations corresponds to the 20% of solutions which have an early, high peak of pro-inflammatory cytokines (see Fig. 2).

Anti-inflammatory cytokines are also produced at a much faster rate in the simulated aged hosts (parameter  $b_{FG}$ ). Aged individuals are known to exhibit a Th2 cytokine phenotype, producing more anti-inflammatory cytokines, such as IL-4 and IL-10, than younger individuals (Ginaldi et al. 2001). Though we do not have anti-inflammatory data to which to fit the equation for the anti-inflammatory cytokine, our model still accurately predicts a higher amount of anti-inflammatory production in the aged ensemble. The adult macaques appear insensitive to this parameter, likely due to the lack of data used to fit that equation.

The simulations showed substantially more damage created in the aged hosts compared to the younger. This corresponds to the higher rates of cell death  $(a_{HF} \text{ and } a_I)$  seen in the elderly host ensemble. Interestingly, the rate of damage healing  $(a_d)$  is higher in the aged macaque ensemble. This parameter difference is largely data driven. Because the aged macaque data hit a much higher peak value of the damage variable than the adults, but still returns to a baseline level of 0 after 14 days, the eradication of damage must be higher in the aged ensemble. However, the increased rate of damage creation outweighs the rate of damage healing, so the aged animals still end up with a much higher proportion of tissue damage.

#### 2.3.2 Younger Animals Control Viral Dynamics More Effectively

Several parameters that govern the viral dynamics also vary between age groups (Fig. 5). Viral replication rate ( $\gamma_V$ ) is about one order of magnitude higher in the elderly macaques, leading to the higher peak values seen in the virus data in Fig. 3. Cellular senescence has been shown to lead to increased viral replication, as senescence can decrease antiviral signaling (Kim et al. 2016; Kelley et al. 2020).

The effector cell-mediated killing of infected cells (parameter  $a_{IE}$ ) is about two orders of magnitude lower in the older macaques. This difference is again supported by experimental data. T cells are dysregulated with age, with a higher percentage of T cells as memory cells rather than effector cells responding to new antigen (Fulop et al. 2020).

Median cell replication (parameter  $b_{HD}$ ) is also lower in the aged hosts, as would be expected, since cell replication rates tend to slow with age (Tomasetti et al. 2019). We do not see a substantial difference in the rate of antibody-mediated viral clearance (parameters  $\alpha_{VU}$  and  $\alpha_{VL}$ ). The virus is cleared from the host around day 14 post-infection, and the antibodies peak between day 14 and day 21 post-infection, so their difference in magnitude does not impact the viral dynamics as much as the nonspecific clearance and the phagocytosis of the infected cells.



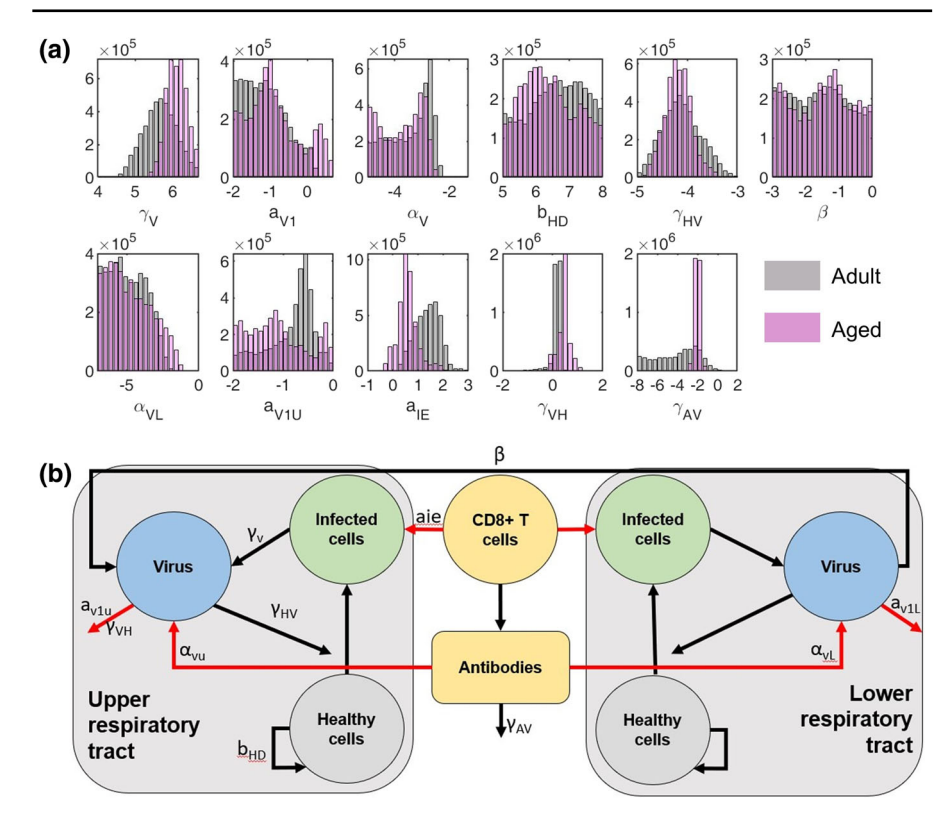


**Fig. 5 a** One-dimensional parameter distributions controlling viral dynamics for adult (black) vs aged (magenta) macaques. **b** Partial network diagram of viral dynamics in the model. For a full description of the variables and parameters, see Methods and Materials

A few parameters do not vary much with age (Figure S1, supplemental materials). Most denominator and saturation parameters, such as  $k_{VFU}$ ,  $k_{VFL}$ , a,  $a_{V2}$ , and w, show very similar distributions between the age groups. Most of the sensitivity and the age-dependent differences in parameter distributions are centered in the inflammatory response, which aligns with our expectations, given the severity of inflammation dysregulation that occurs with aging. Figures S2 and S3 (Supplemental Materials) show the pairwise correlations between parameters in the adult and aged ensembles, respectively.

## 2.4 Simulating Dynamics of T cell Dysfunction Demonstrates Likelihood of Increased Morbidity and Mortality Due to Excess Viral Titers

Viral peptides stimulate the CD8<sup>+</sup> T cell response when presented by class I major histocompatibility complex molecules on the infected epithelial cells (Cannon et al. 1988). Persistent stimulation can lead to T cell exhaustion, limiting the efficacy of the adaptive immune responses and increasing the morbidity and mortality associated



with an infection. T cell exhaustion is often linked with persistent infections, such as lymphocytic choriomeningitis (LCMV) (Gallimore et al. 1998) or HIV (Day et al. 2006), and also with chronic conditions such as sepsis (Inoue et al. 2014; Saito et al. 2020) or cancer (Pauken and Wherry 2015). In addition to these chronic conditions, T cell exhaustion has also been shown to occur after severe influenza infection with prolonged antigen stimulation (Bucks et al. 2009) as well as COVID-19 (Westmeier et al. 2020). Exhausted T cells demonstrate decreased cytolytic activity, which can make the infection more severe and limit the host's ability to clear the virus effectively.

A wide range of preexisting conditions and disorders can cause T cell dysfunction. Aging naturally leads to T cell dysfunction (Ferrando-Martínez et al. 2013), and immunocompromised patients may experience partial or full T cell dysfunction as well (Liston et al. 2008). Previous experimental studies show that T cell dysfunction and dysregulation are associated with highly pathogenic influenza infections (Rutigliano et al. 2014). We have shown that this mathematical model accurately reproduces dynamics after influenza and COVID-19 infection. We now use this model to replicate clinically relevant host conditions like T cell exhaustion to further demonstrate that this model can be widely applicable in viral infection modeling. Changing parameters controlling the magnitude and efficacy of the T cell response can qualitatively demonstrate the way in which our model responds to changes in the T cell population, which occur naturally with age and can also affect a host long after exposure to a severe or chronic infection.

## 2.4.1 Simulation of T cell Dysfunction in Young and Older Macagues

To demonstrate the effect of T cell dysfunction and dysregulation on our parameter ensembles, we adjusted parameters which control T cell activation and efficacy and assessed whether our model would predict survival or death after forced T cell exhaustion. Three total parameters were changed in this analysis: the rate at which effector cells kill infected cells (parameter  $a_{IE}$ ), the rate at which the presence of virus will lead to the recruitment of T cells (parameter  $\gamma_{\rm EV}$ ), and the rate at which cellular damage will lead to the recruitment of T cells (parameter  $\gamma_{ED}$ ). These parameters were multiplied by a value between 0 and 1, where multiplying by 1 will recreate the original fits to the data, and multiplying by 0 will essentially turn off the corresponding mechanism of the immune response. Because two of these parameters control the stimulation of the effector cells (parameters  $\gamma_{ED}$  and  $\gamma_{EV}$ ), we changed both parameters simultaneously to control the effector cell activation. Parameter  $\alpha_{IE}$  was changed independently of the other two, as it controls an independent mechanism. We performed this systematic parameter adjustment on all parameter sets included in the ensemble of models shown in Figs. 2 and 3. All initial conditions and remaining parameters were kept identical to those used in the original fits to the data, and the model was simulated for 100 dpi to assess the end behavior of the trajectories.

Figure 6 shows the results of this experiment, focusing on the likelihood of survival at various degrees of T cell disability. Each cell in the heatmap indicates the average final value of the epithelial cells in the upper (left heatmaps) and lower (right heatmaps) compartments across all parameter sets contained in the ensembles. In the upper compartment, healthy cells have a maximum value of 0.33. If these cells can



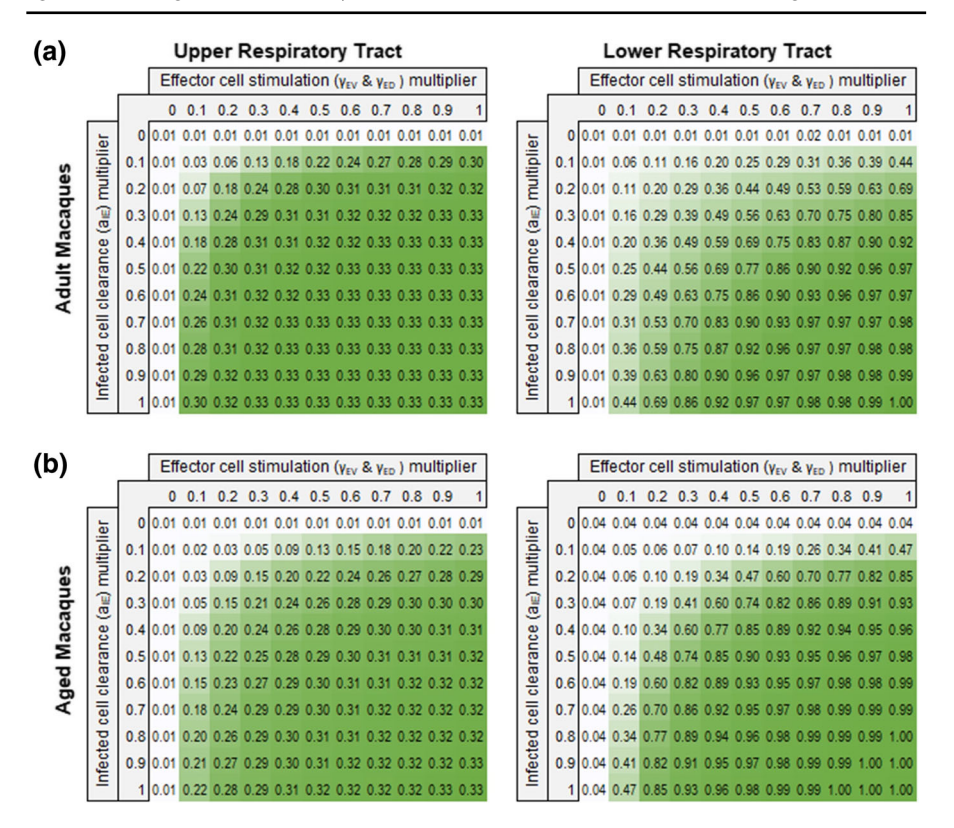


Fig. 6 Simulation of T cell dysfunction in  $\bf a$  adult and  $\bf b$  aged macaque ensembles. The stimulation of the T cell activation (parameters  $\gamma_{\rm ED}$  and  $\gamma_{\rm EV}$ ) and the effector cell activity (parameter  $a_{IE}$ ) were systematically decreased to simulate varying levels of T cell dysfunction in young and older hosts. A simulation is considered survivable if healthy cells in the lower respiratory compartment return to their baseline level ( $H_{\rm L}$ =1.00). Simulations were repeated for all parameter sets in each ensemble, and the value displayed in each heatmap is the average final value of  $H_{\rm L}$  across all simulations. The color in the heatmap is proportional to the final value of  $H_{\rm L}$ ; the darker the color, the more healthy cells are predicted to remain at the end of the simulation

return to their baseline level of 0.33 by the end of the simulation, then the model predicts the host suffers no lasting damage to the upper respiratory tract.

In the lower compartment, healthy cells have a maximum value of 1.00. If healthy cells in the lower respiratory tract return to their baseline level of 1.00 (representing a state of no infected cells present in the lungs and full recovery of the healthy epithelial cell population), then the model predicts that the parameter set leads to survival of the host. The death state in this model is defined by depletion of epithelial cells in the lower respiratory tract, so simulations that end with zero healthy cells remaining in the lower compartment correspond to simulations that predict death of the host. Each value in the heatmap represents an average across the ensemble, representing a likelihood of survival or death following the indicated level of T cell dysfunction. The lower the value in the cell, the more likely that the model predicts the host would die under those conditions. The saturation of the color in each cell is proportional



to the value in the cell; darker colors correlate to higher percentage of healthy cells remaining at the end of the simulation.

Unsurprisingly, keeping T cell parameters near their initial values (setting multipliers at or near 1, lower right corners of the heatmaps) generally results in a favorable outcome for the host, given that these ensembles were originally used to simulate dynamics in a survivable infection. As these T cell-related parameters decrease (towards the upper left corners of the heatmaps), the likelihood of host death increases (as the percent of remaining healthy cells in the lower compartment decreases). When  $a_{IE}$  (infected cell clearance) is set to 0, the host is generally unable to resolve the infection and death is predicted (healthy cells have a final value of 0 for nearly every simulation), regardless of the other parameters in the model. This implies that almost all parameter sets in the ensemble rely heavily on the T cells to control the infected cell population and limit viral replication.

Lowering the T cell stimulation (parameters  $\gamma_{ED}$  and  $\gamma_{EV}$ ) also decreases the likelihood of host survival (left side of each heatmap). With lower T cell stimulation, fewer T cells can react to the infection, and the virus will replicate too quickly for the remaining immune responses to compensate. Setting both terms to 0 (upper left corner) is functionally equivalent to a full T cell knockout, which leads to death in over 99% of simulated cases.

Overall, the aged ensemble is more susceptible to death via T cell exhaustion than the adult ensemble. In both the upper and the lower respiratory tracts, more parameter sets predict the healthy cells will be eradicated, leading to death or chronic upper respiratory symptoms and damage. T cells undergo major changes with age, including a shift in the T cell population to include more memory T cells and fewer effector T cells (Wick et al. 2000). This dysregulation is compounded by the decreased effector functions created in this experiment, leading to an increased likelihood of morbidity and mortality in the elderly ensemble.

## 2.4.2 Survival After T cell Exhaustion Requires Strong Infected Cell Clearance via Innate Immunity

We next sought to identify what mechanisms or immune components are most closely tied to survival or death after T cell exhaustion. Using the heatmaps in Fig. 6, we identified multipliers that would lead to about 50% survival in our ensemble. For the adult ensemble, we multiplied the effector cell stimulation by 0.3 and infected cell clearance by 0.4. (Fig. 6 indicates that about 49% of the ensemble survived the T cell exhaustion under those conditions.) We solved the system of ODEs with each parameter set in the ensemble, with the stated changes to effector cell stimulation and infected cell clearance. Each parameter set was then classified as either a "survivor" or "non-survivor," based on whether the healthy cells in the lower compartment had depleted at the end of the simulation.

We analyzed the parameter distributions between the survivors and non-survivors to identify which components of the immune response may differ most between these two groups. While many parameters' distributions were not statistically different from one another, a few parameters do stand out as different by inspection between phenotypes. In the adult ensembles (Fig. 7), individuals that survived tended to have higher values



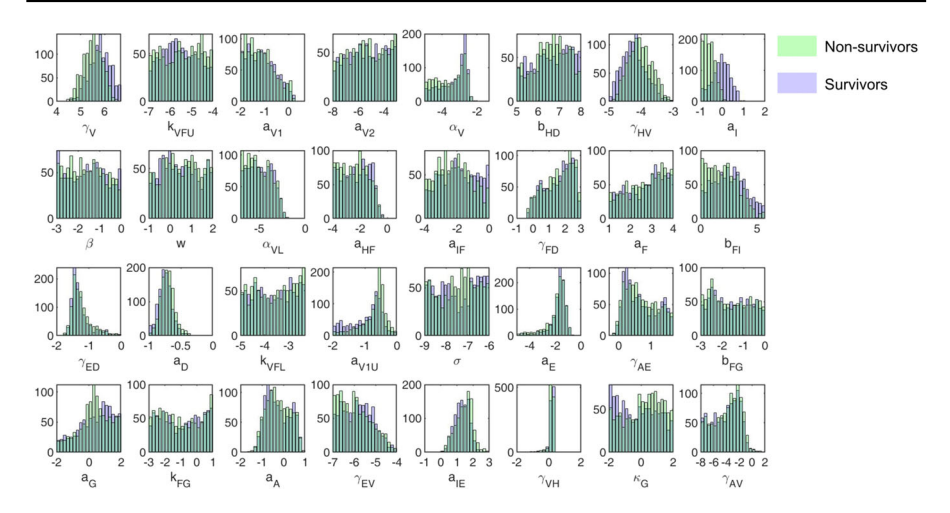


Fig. 7 Parameter distributions from adult survivors (blue) and non-survivors (green) of simulated T cell exhaustion. Adult hosts that can survive T cell exhaustion tend to exhibit stronger stimuli to the immune response, leading to stronger compensatory mechanisms to clear the virus and survive the infection. Parameters  $\gamma_V$ ,  $\gamma_{HV}$ ,  $\alpha_I$ , and  $b_{F1}$  all tend to be higher in the surviving ensembles

of  $a_I$  (natural death rate of infected cells),  $\gamma_V$  (viral replication), and  $\gamma_{HV}$  (viral internalization by epithelial cells) and  $b_{FI}$  (production of inflammation by stimulation from infected cells). These parameter trends indicate that a host is more likely to survive an episode of T cell exhaustion if infected cells die out more quickly or if the virus grows more slowly, as both trends would yield a more manageable infection dynamic. In the aged ensemble (Fig. 8), few parameters are visibly different between sur-

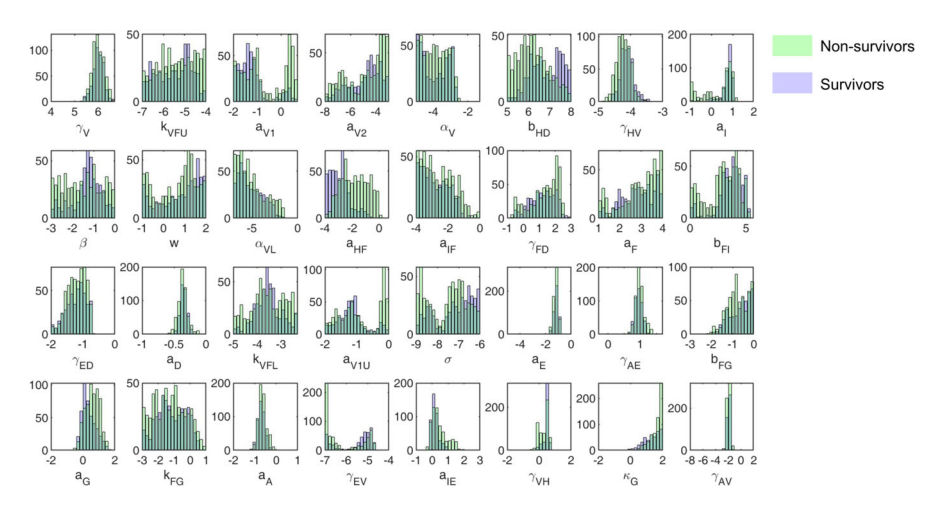


Fig. 8 Parameter distributions from aged survivors (blue) and non-survivors (green) of simulated T cell exhaustion. Aged hosts that can survive T cell exhaustion tend to have better control over epithelial cell replication ( $b_{HD}$ , top row, panel 6) and inflammation-induced cell death ( $\alpha_{HF}$ , middle row, panel 4)



**88** Page 16 of 24 E. Mochan et al.

vivors and non-survivors. The ensembles reveal that only hosts with resilient epithelial cells will be able to survive T cell exhaustion. Survivors tend to have higher rates of epithelial cell replication (parameter  $b_{HD}$ ) and lower rates of inflammation-induced cell death ( $\alpha_{HF}$ ). Taken together, these parameters diminish cell death, which increases the likelihood of host survival.

## 2.4.3 Increased Levels of IL-15 Can Reverse T cell Dysfunction and Promote Survival

A study by Saito et al. (Saito et al. 2020) demonstrated that the severe T cell exhaustion seen in elderly patients could be reversed through stimulation of the T cells with IL-15. The pro-inflammatory mediator (F) in our model was fitted to IL-15 data, so by increasing the stimulation of IL-15, we can simulate similar experimental conditions to again verify that our model can replicate clinically relevant immunodynamics related to host survival after severe infection.

To test our model's response to increased IL-15 after simulated T cell dysregulation, we again systematically changed our calibrated parameters to allow for an amplified pro-inflammatory signal. An increase in the parameter  $b_{FI}$  represents an increase in inflammation due to the presence of infected cells, and an increase in the parameter  $\gamma_{FD}$  represents an increase in inflammation due to sensing of cellular damage. Increasing either of these parameter values will increase F in our model.

We tested whether our model could predict the survival of some lethal cases of T cell exhaustion through an increase in IL-15. We took the parameter sets labeled as "non-survivors" in Figs. 7 and 8 and increased parameters  $b_{FI}$  and  $\gamma_{FD}$  by orders of magnitude to assess by how much the IL-15 response needs to be adjusted to transform a predicted lethal case into a survivable case. As Fig. 9 shows, this is possible for both adult and aged hosts.

Outcomes for the subset of non-survivors of T cell exhaustion are much more sensitive to parameter  $\gamma_{FD}$  than to parameter  $b_{FI}$ ; the final number of healthy cells in either compartment does not change much as  $b_{FI}$  increases, demonstrated by the consistency in the end value of the healthy cells within a single row of the heatmaps in Fig. 9. Changes in  $b_{FI}$  only seem to make a difference in the survival rate when parameter  $b_{FI}$  is relatively low. Large increases in  $b_{FI}$  will lead to survival for most simulations with a fairly low value of  $b_{FI}$ . These results imply that our subset of non-survivors of T cell exhaustion are unlikely to die from an excess of inflammation due to the presence of infected cells. However, this scenario would lead to an extremely high peak in both damage and inflammation, likely leading to severe sepsis and symptoms for the host.

Some interesting dynamics arise as the damage-dependent stimulation of inflammation is changed. As  $\gamma_{FD}$  increases, the likelihood of host survival initially increases as well. However, multiplying  $\gamma_{FD}$  by large numbers will eventually have a detrimental effect on the host, as the survival rate begins to diminish towards the bottom half of the heatmaps. The damage equation was fitted to data for IL-6, and high levels of IL-6 are known to be a strong indicator of morbidity and mortality (Ginaldi et al. 2001). Clearly, the damage-dependent pathway to stimulate inflammation can be detrimental to a host with a diminished T cell response.



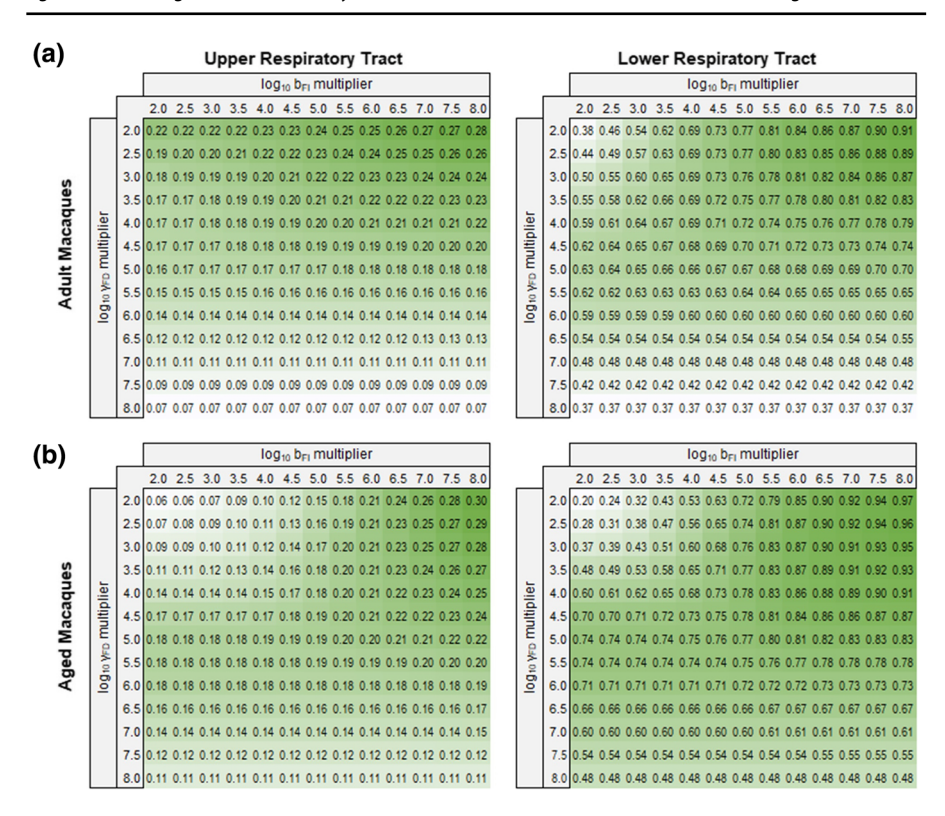


Fig. 9 Survival after simulated T cell dysregulation due to IL-15 stimulation for (a) adult and (b) aged macaques. Lethal T cell exhaustion was induced through parameter changes (see Sect. 2.4.2 for details, and Figs. 7 and 8). These lethal conditions were then updated to induce an increased pro-inflammatory response to determine whether IL-15 can reverse lethal T cell dysfunction. The pro-inflammatory response was upregulated by increasing parameter  $b_{FI}$  and/or parameter  $\gamma_{FD}$ , both of which produce higher levels of F in the model. A simulation is considered survivable if healthy cells in the lower respiratory compartment return to their baseline level ( $H_L$ =1.00). The value displayed in each heatmap is the average final value of  $H_L$  across all simulations. The color in the heatmap is proportional to the final value of  $H_L$ ; the darker the color, the more healthy cells are predicted to remain at the end of the simulation. The patterns shown in these heatmaps indicate that as parameter  $\gamma_{FD}$  increases, the survival rate initially improves, but if  $\gamma_{FD}$  gets too large, the survival rate begins to diminish again, indicating that excess damage is a lethal side effect of increased IL-15

#### 3 Discussion

In the present study, we further develop and explore a recently proposed ODE model of the immune response to respiratory viral infection (Mochan et al. 2021). We show that this model can accurately replicate data influenza infection, making our model broadly applicable to viral infection data. The model identifies differences in immune response to influenza infection between young adult and aged hosts due to age-induced immune dysregulation (Figs. 4 and 5). Our model can also accurately replicate dynamics associated with T cell dysfunction (Fig. 6) and can even simulate therapeutic effects to offset the deleterious effects of T cell dysfunction (Fig. 9). The experimental data



to which our model was fit showed a more severe infection in the elderly macaques compared to the younger adults. Aged animals had higher viral loads in both upper and lower compartments, and a significantly higher inflammatory response, especially at day 4 post-infection.

While all model parameters were permitted to vary between age groups, a small subset of parameters stand out as varying greatly between young and older hosts. In particular, the parameters governing the inflammatory response show significant differences between age groups. The older animals demonstrated a stronger proinflammatory response, indicated by the higher values for parameters controlling production of IL-15 and tissue damage creation. Older animals also showed a higher rate of viral replication and lower effector cell action, contributing to the higher viral titers in the aged macaque data. The experimental data for measured CD8 + T cells were not substantially different between older and younger hosts, but the ensemble still captured differences in the parameters governing the T cell trajectory.

We have also demonstrated the clinical relevance of this model by showing its ability to replicate dynamics of infection-induced T cell exhaustion. We have shown that T cell exhaustion is not necessarily lethal, though it can certainly exacerbate the infection. Reversal of T cell exhaustion has been proven experimentally with an influx of IL-15 (Saito et al. 2020). This model can replicate that behavior with simple parameter changes which strengthen the pathways stimulating the inflammatory response. Our model includes two independent pathways leading to an increase in inflammation: one stimulated by the presence of infected cells (parameter  $b_{FI}$ ) and one stimulated by the presence of cellular damage ( $\gamma_{FD}$ ). We determined that the damage-dependent pathway can positively impact the survival after T cell exhaustion to a point, but further stimulation of that pathway can then negatively impact the host and diminish the chances of survival. Tissue damage will last longer than the population of infected cells, so balancing their effects on the production of inflammation is critical to controlling this positive feedback loop. We theorize that finding this balance is key to balancing the immune response which can precisely target and repair the infected cells, but imprecisely target tissue damage.

The production of inflammation in our model is of course a simplification of the true biological interactions and dynamics involved in this complex cascade of proinflammatory signals. The term  $b_{FI}I$  represents a fast-acting signaling pathway from the detection of the presence of infected epithelial cells to the production of proinflammatory mediators, such as type I interferon, by nearby cells. Our simulations of the reversal of T cell exhaustion (Fig. 7) clearly demonstrate the importance of emphasizing the fast-acting signaling pathway driven by infected cells, rather than the damage-dependent pathway. Our model is not detailed enough to identify the exact pathway, but this certainly presents an important avenue for future experimental work.

Future work may also include adding further detail to our approach to the modeling of T cell exhaustion to allow for a more dynamic change in T cell activation and efficacy. Our current approach decreases the parameters controlling T cell behavior by a static percentage across the entire time course of the simulation. Future iterations of the model may include additional parameters or equations to allow the T cell exhaustion to turn on and off at certain time points, or dynamically build as antigen exposure increases over time.



The ensemble model is useful in accommodating uncertainty in experimental data, but it does require some simplifying assumptions which create limitations of the approach. Our model presumes that the upper and lower respiratory compartments are well-mixed. This is, of course, a simplification of the true biology; in reality, there is a spatial component to the viral plaque growth and spread which impacts its replication in the host (Sego et al. 2020). Future iterations of this work may include a multiscale approach to include this spatial heterogeneity in addition to our time-dependent dynamics. We also do not have experimental data to which to fit the epithelial cell populations or the latter half of several of the measured variables, so our fits transition to predictions after 2 weeks post-infection. Experimental datasets with this level of longitudinal detail do not currently exist, so our model may serve as a mechanism for understanding these details that are not currently being experimentally measured.

In conclusion, we have demonstrated the versatility of this model by fitting it to datasets for two age groups infected with H1N1. While a substantial number of parameters vary between age groups, those controlling the inflammatory response and direct viral clearance were most disparate between the old and young hosts. In addition, our model can replicate clinically relevant conditions like T cell exhaustion, as well as the reversal of this exhaustion by inducing IL-15 production.

#### 4 Methods and Materials

#### 4.1 Model Structure

The equations of the ODE model are given in (1)-(11). We have adapted our previous ODE model (Mochan et al. 2021), adding two equations to incorporate the adaptive immune response. The model incorporates two compartments: the upper respiratory tract (modeled in Eqs. (1)-(3), with variables and parameters with subscript U), and the lower respiratory tract (modeled in Eqs. (4)-(6), with variables and parameters with subscript L). The remaining equations represent components that are not contained to a single compartment, but rather affect the host globally.

In summary, the virus (V) is released by infected cells (I) and is cleared by nonspecific immunity  $(\alpha_{VU} \text{ and } \alpha_{VL})$  or by antibodies (A) at rate  $\alpha_{VU}$  or  $\alpha_{VL}$ . The virus can move from the lower compartment to the upper via the mucociliary elevator. As healthy cells (H) interact with the virus, they become infected, and the presence of infected cells stimulates the inflammatory response (F). Sustained inflammation leads to cellular damage (D) and activation of the anti-inflammatory mediator (G). A table of all parameters and their biological interpretation is given in the Supplemental Materials (Table S1).

Equation (10) gives the dynamics for the CD8<sup>+</sup> T cell response. T cells are stimulated by the presence of damage and virus in either compartment, but they are limited in their efficacy by the anti-inflammatory cytokine, G. T cells decay naturally on the order of days (Schlub et al. 2011). T cells act as effector cells, killing infected cells in both the upper and lower compartments at rate  $a_{IE}$  (Eqs. (3) and (6)). This additional source of cell death also adds to the cumulative tissue damage in the system (Eq. (8)).



**88** Page 20 of 24 E. Mochan et al.

Equation (11) gives the dynamics for the antibody response. The humoral response begins after the T cells have been activated. Antibodies decay naturally and are depleted when they attach to virus to remove it from the system. Antibodies kill the virus in both the upper and lower compartments (parameters  $\alpha_{VU}$  and  $\alpha_{VL}$ , respectively).

$$\frac{dV_{U}}{dt} = \frac{\gamma_{V} I_{U} f(V_{U}, \varepsilon_{V})}{1 + \kappa_{VFU} F} - \gamma_{VH} H_{U} V_{U} - \alpha_{VU} V_{U} A - \frac{a_{VU} V_{U}}{1 + a_{V2} V_{U}} + \frac{\beta V_{L}}{1 + w V_{L}}$$
(1)

$$\frac{dH_U}{dt} = b_{HD}(H_{\text{max}} - H_U - I_U)H_U\left(\frac{H_U - \varepsilon}{H_{U} + \varepsilon}\right) - \gamma_{HV}V_UH_U - a_{HF}FH_U \quad (2)$$

$$\frac{dI_U}{dt} = \gamma_{HV} V_U H_U - a_{IF} F I_U - a_I I_U - a_{IE} I_U E \tag{3}$$

$$\frac{dV_L}{dt} = \frac{\gamma_V I_L f(V_L, \varepsilon_V)}{1 + \kappa_{VFL} F} - \gamma_{VH} H_L V_L - \alpha_{VL} V_L A - \frac{a_{VL} V_L}{1 + a_{V2} V_L} - \frac{\beta V_L}{1 + w V_L}$$
(4)

$$\frac{dH_L}{dt} = b_{HD}(H_{\text{max}} - H_L - I_L)H_L\left(\frac{H_L - \varepsilon}{H_I + \varepsilon}\right) - \gamma_{HV}V_LH_L - a_{HF}FH_L \quad (5)$$

$$\frac{dI_L}{dt} = \gamma_{HV} V_L H_L - a_{IF} F I_L - a_I I_L - a_{IE} I_L E \tag{6}$$

$$\frac{dF}{dt} = \frac{\gamma_{FD}D + b_{FI}(I_U + I_L)}{1 + k_{FG}G} - a_F F \tag{7}$$

$$\frac{dD}{dt} = \frac{(\Sigma_D)^m}{1 + \sigma(\Sigma_D)^m} - a_D D \tag{8}$$

$$\frac{dG}{dt} = \gamma_{FG}F - a_GG \tag{9}$$

$$\frac{dE}{dt} = \frac{\gamma_{ED}D + \gamma_{EV}(V_U + V_L)}{1 + \kappa_E G} - a_E E \tag{10}$$

$$\frac{dA}{dt} = \gamma_{AE}E - a_aA - \gamma_{AV}(V_U + V_L) \tag{11}$$

$$f(V, \varepsilon_V) = \frac{V(V - \varepsilon_V)}{(V + \varepsilon_V)^2}$$

$$\Sigma_D = a_{HF}F(H_U + H_L) + a_{IF}F(I_U + I_L) + a_I(I_U + I_L) + a_{IE}(I_U + I_L)$$

## 4.2 Experimental data

Experimental data for these fits were taken from Josset et al. (Josset et al. 2012). In these experiments, 16 female rhesus macaques were infected with the 2009 H1N1 strain CA04, which was derived from the 2009 swine flu pandemic. Eight macaques



were age 10–12 years old, considered to be young adults, and eight macaques were 20–24 years old, considered to be aged. These animals had no preexisting immunity against the virus. Virus was administered via intranasal, intratracheal, and intraocular routes, with four times as much virus administered intratracheally as was administered intranasally. Viral titers were measured 0, 4, 7, 10, 14, and 21 days post-infection (dpi). Blood samples were also collected on these days, as well as days 28, 35, 77, and 99. Overall, these data showed that, compared to younger animals, aged animals exhibit higher viral titers, higher hemagglutination inhibition (HI) titers, and higher peak values of pro-inflammatory cytokines.

We used IL-15 data as a proxy for inflammation, in accordance with our previous work (Mochan et al. 2021). In addition, we used IL-6 data as a proxy for damage, as IL-6 is one of the first cytokines released in response to damage (Jawa et al. 2011), and high levels of IL-6 are a major predictor of host morbidity and mortality after infection (Ginaldi et al. 2001).

Initial conditions used in our simulations were derived from these experimental conditions.  $V_U(0) = 100$ ,  $V_L(0) = 400$ , and all other variables were assumed to start at their natural baseline state if no infection was present. Infected cells, damage, proand anti-inflammatory cytokines, T cells, and antibodies all begin at an initial value of 0. Healthy cells begin at their maximum value (0.33 in the upper compartment and 1.00 in the lower compartment).

## 4.3 Data fitting with Monte Carlo sampling

The model presented here consists of 11 equations comprised of 32 parameters. To evaluate the uncertainty in estimation of parameter values of the model, we apply a Bayesian inference approach together with Markov chain Monte Carlo sampling to determine a posterior distribution of the parameters (Mochan et al. 2014; Mochan-Keef et al. 2015; Price et al. 2015). The likelihood function used to create the posterior distribution is the exponential of the negative sum of squared errors:

$$L(y|\mathbf{p}) = \exp\left(-\sum_{i,j} \frac{\left(\overline{y}_{i,j} - y_{i,j}\right)^2}{2\sigma_{i,j}^2}\right)$$

where p is the vector of all parameters of the system, y represents the experimental data for variable j at time i,  $\overline{y}_{i,j}$  is the mean of variable j at time i, and  $\sigma_{i,j}^2$  is the standard deviation of the variable.

We select a Jeffreys prior distribution for each parameter, which is a uniform distribution on a log scale, within biologically reasonable estimated bounds on each parameter. At each step of the simulation, a new 32-dimensional parameter set is generated and the error is calculated for the trajectories that parameter set creates. To explore this parameter space thoroughly, we simulated four million parameter sets within these bounds. The parameter ensembles were then analyzed to identify trends in the fits to the data. The resulting marginal distributions are shown in Figs. 4, 5, and S1. These graphs define the probabilities of parameters taking on particular values



**88** Page 22 of 24 E. Mochan et al.

within their pre-defined bounds; the more parameter sets that contain a certain value, the more likely it is that the parameter would assume that value within the population.

Supplementary Information The online version contains supplementary material available at https://doi.org/10.1007/s11538-022-01045-z.

**Acknowledgements** T.J.S. acknowledges funding from National Institutes of Health grants U24 EB028887 and R01 GM122424 and National Science Foundation grant NSF 1720625. B.E. acknowledges funding from the National Science Foundation 1951099.

Data availability Data will be made available upon reasonable request.

### References

- Baral S, Antia R, Dixit NM (2019) A dynamical motif comprising the interactions between antigens and CD8 T cells may underlie the outcomes of viral infections. Proc Natl Acad Sci USA 116:17393–17398. https://doi.org/10.1073/pnas.1902178116
- Bourgeois MA, Oaks JL (2014) Chapter 12 Laboratory Diagnosis of Viral Infections. In: Equine Infectious Diseases (Second Edition). pp 132–140
- Bucks CM, Norton JA, Boesteanu AC et al (2009) Chronic antigen stimulation alone is sufficient to drive CD8 + T cell exhaustion. J Immunol 182:6697–6708. https://doi.org/10.4049/jimmunol.0800997
- Cannon MJ, Openshaw PJ, Askonas BA (1988) cytotoxic t cells clear virus but augment lung pathology in mice infected with respiratory syncytial virus. Cell 168:1163–1168
- Day CL, Kaufmann DE, Kiepiela P et al (2006) PD-1 expression on HIV-specific T cells is associated with T-cell exhaustion and disease progression. Nature 443:350–354
- Ferrando-Martínez S, Romero-Sánchez MC, Solana R et al (2013) Thymic function failure and C-reactive protein levels are independent predictors of all-cause mortality in healthy elderly humans. Age (omaha) 35:251–259. https://doi.org/10.1007/s11357-011-9341-2
- Franceschi C, Bonafè M, Valensin S et al (2000) Inflamm-aging. an evolutionary perspective on immunosenescence. Ann N Y Acad Sci 908:244–254. https://doi.org/10.1111/j.1749-6632.2000.tb06651.x
- Franceschi C, Bonafè M, Valensin S (2000b) Human immunosenescence: the prevailing of innate immunity, the failing of clonotypic immunity, and the filling of immunological space. Vaccine 18:1717–1720
- Fulop T, Witkowski JM, Olivieri F, Larbi A (2018) The integration of inflammaging in age-related diseases. Semin Immunol 17:35
- $Fulop\ T, Larbi\ A, Hirokawa\ K\ et\ al\ (2020)\ Immunosenescence\ is\ both\ functional\ /\ adaptive\ and\ dysfunctional\ /\ maladaptive.\ Semin\ Immunopathol\ 42:521-536$
- Gallimore A, Glithero A, Godkin A et al (1998) Induction and exhaustion of lymphocytic choriomeningitis class I peptide complexes. J Exp Med 187:1383–1393
- Ginaldi L, Loreto MF, Corsi MP et al (2001) Immunosenescence and infectious diseases. Microbes Infect 3:851–857
- Inoue S, Suzuki K, Komori Y et al (2014) Persistent inflammation and T cell exhaustion in severe sepsis in the elderly. Crit Care. https://doi.org/10.1186/cc13941
- Jawa RS, Anillo S, Huntoon K et al (2011) Interleukin-6 in surgery, trauma, and critical care: part I: basic science. J Intensive Care Med 26:3–12
- Josset L, Engelmann F, Haberthur K et al (2012) Increased viral loads and exacerbated innate host responses in aged macaques infected with the 2009 pandemic H1N1 influenza a virus. J Virol 86:11115–11127. https://doi.org/10.1128/jvi.01571-12
- Kahan SM, Wherry EJ, Zajac AJ (2015) T cell exhaustion during persistent viral infections. Virology 479–480:180–193. https://doi.org/10.1016/j.virol.2014.12.033
- Keef E, Zhang LA, Swigon D et al (2017) Discrete dynamical modeling of influenza virus infection suggests age-dependent differences in immunity. J Virol 91:1–18. https://doi.org/10.1128/jvi.00395-17
- Kelley WJ, Zemans RL, Goldstein DR (2020) Cellular senescence: Friend or foe to respiratory viral infections? Eur Respir J. https://doi.org/10.1183/13993003.02708-2020
- Kim JA, Seong RK, Shin OS (2016) Enhanced viral replication by cellular replicative senescence. Immune Netw 16:286–295. https://doi.org/10.4110/in.2016.16.5.286



- Kopf M, Baumann H, Freer G et al (1994) Impaired immune and acute-phase responses in interleukin-6-deficient mice. Nature 368:339–342. https://doi.org/10.1038/368339a0
- Liston A, Enders A, Siggs OM (2008) Unravelling the association of partial T-cell immunodeficiency and immune dysregulation. Nat Rev Immunol 8:545–558. https://doi.org/10.1038/nri2336
- Meyer KC (2001) The role of immunity in susceptibility to respiratory infection in the aging lung. Respir Physiol 128:23–31
- Mochan E, Swigon D, Ermentrout GBB et al (2014) A mathematical model of intrahost pneumococcal pneumonia infection dynamics in murine strains. J Theor Biol 353:44–54. https://doi.org/10.1016/j. jtbi.2014.02.021
- Mochan E, Sego TJ, Gaona L et al (2021) Compartmental model suggests importance of innate immune response to COVID - 19 infection in rhesus macaques. Bull Math Biol. https://doi.org/10.1007/s11538-021-00909-0
- Mochan-Keef E, Swigon D, Ermentrout GBB, Clermont G (2015) A three-tiered study of differences in murine intrahost immune response to multiple pneumococcal strains. PLoS ONE 10:e0134012. https://doi.org/10.1371/journal.pone.0134012
- Moskophidis D, Lechner F, Pircher H, Zinkernagel RM (1993) Virus persistence in acutely infected immunocompetent mice by exhaustion of antiviral cytotoxic effector T cells. Nature 362:758–761. https://doi. org/10.1038/362758a0
- Pauken KE, Wherry EJ (2015) Overcoming T cell exhaustion in infection and cancer. Trends Immunol 36:265–276. https://doi.org/10.1016/j.it.2015.02.008.Overcoming
- Plowden J, Renshaw-Hoelscher M, Engleman C et al (2004) Innate immunity in aging: impact on macrophage function. Aging Cell 3:161–167. https://doi.org/10.1111/j.1474-9728.2004.00102.x
- Price I, Mochan-Keef ED, Swigon D et al (2015) The inflammatory response to influenza A virus (H1N1): an experimental and mathematical study. J Theor Biol 374:83–93. https://doi.org/10.1016/j.jtbi.2015.03.017
- Rutigliano JA, Sharma S, Morris MY et al (2014) Highly pathological influenza a virus infection is associated with augmented expression of PD-1 by functionally compromised virus-specific CD8+ T cells. J Virol 88:1636–1651. https://doi.org/10.1128/jvi.02851-13
- Saito M, Inoue S, Yamashita K et al (2020) IL-15 improves aging-induced persistent T cell exhaustion in mouse models of repeated sepsis. Shock 53:228–235
- Salminen A, Kaarniranta K, Kauppinen A (2012) Inflammaging: disturbed interplay between autophagy and inflammasomes. Aging (Albany NY) 4:166–175
- Schlub TE, Sun JC, Walton SM et al (2011) Comparing the kinetics of NK Cells, CD4, and CD8 T cells in murine cytomegalovirus infection. J Immunol 187:1385–1392. https://doi.org/10.4049/jimmunol. 1100416
- Sego TJ, Aponte-Serrano JO, Ferrari Gianlupi J, Heaps SR, Breithaupt K, Brusch L, Glazier JA (2020) A modular framework for multiscale, multicellular, spatiotemporal modeling of acute primary viral infection and immune response in epithelial tissues and its application to drug therapy timing and effectiveness. PLoS Comput Biol 16(12):e1008451
- Shaw AC, Joshi S, Greenwood H et al (2010) Aging of the innate immune system. Curr Opin Immunol 22:507–513. https://doi.org/10.1016/j.coi.2010.05.003
- Toapanta FR, Ross TM (2009) Impaired immune responses in the lungs of aged mice following influenza infection. Respir Res 10:112–131. https://doi.org/10.1186/1465-9921-10-112
- Tomasetti C, Poling J, Roberts NJ et al (2019) Cell division rates decrease with age, providing a potential explanation for the age-dependent deceleration in cancer incidence. Proc Natl Acad Sci U S A 116:20482–20488. https://doi.org/10.1073/pnas.1905722116
- Weksler MC, Innes JD, Goldstein G (1978) Immunological studies of aging. IV. the contribution of thymic involution to the immune deficiencies of aging mice and reversal with thymopoietin32-36. J Exp Med 148:996–1006
- Westmeier J, Paniskaki K, Karaköse Z et al (2020) Impaired cytotoxic CD8+ T cell response in elderly COVID-19 patients. Mbio 11:1–14. https://doi.org/10.1101/2020.08.21.262329
- Wick G, Jansen-Dürr P, Berger P et al (2000) Diseases of aging. Vaccine 18:1567–1583. https://doi.org/10. 1016/S0264-410X(99)00489-2
- Yeh E, Luo RF, Dyner L et al (2010) Preferential lower respiratory tract infection in swine-origin 2009 A(HINI) influenza. Clin Infect Dis 50:391–394. https://doi.org/10.1086/649875
- Zajac AJ, Blattman JN, Murali-Krishna K et al (1998) Viral immune evasion due to persistence of activated T cells without effector function. J Exp Med 188:2205–2213. https://doi.org/10.1084/jem.188.12.2205



88 Page 24 of 24 E. Mochan et al.

Zhou H, Thompson WW, Viboud CG et al (2012) Hospitalizations associated with influenza and respiratory syncytial virus in the United States, 1993–2008. Clin Infect Dis 54:1427–1436. https://doi.org/10.1093/cid/cis211

**Publisher's Note** Springer Nature remains neutral with regard to jurisdictional claims in published maps and institutional affiliations.

